

Supplementary Information

Lowering the Cu-O bond energy in CuO nanocatalysts enhances the efficiency of NH₃ oxidation

Lu Chen^{1,2,3*}, Xuze Guan², Zhangyi Yao², Shusaku Hayama⁴, Matthijs A. van Spronsen⁴, Burcu Karagoz⁴, Georg Held⁴, David G. Hopkinson⁵, Christopher S. Allen^{5,6}, June Callison⁷, Paul J. Dyson^{8,*}, Feng Ryan Wang^{2,*}

1. Low-Carbon Conversion Science and Engineering Center, Shanghai Advanced Research Institute, Chinese Academy of Sciences, 201210, Shanghai, China
2. Department of Chemical Engineering, University College London, Roberts Building, Torrington Place, WC1E 7JE, London, United Kingdom
3. Yusuf Hamied Department of Chemistry, University of Cambridge, CB2 1EW, Cambridge, United Kingdom
4. Diamond Light Source Ltd., Harwell Science and Innovation Campus, Chilton, OX11 0DE, Didcot, United Kingdom
5. electron Physical Science Imaging Centre, Diamond Light Source Ltd., OX11 0DE, Didcot, United Kingdom
6. Department of Materials, University of Oxford, OX1 3PH, Oxford, United Kingdom
7. UK Catalysis Hub, Research Complex at Harwell (RCaH), Rutherford Appleton Laboratory, OX11 0FA, Harwell, United Kingdom
8. Institute of Chemical Sciences and Engineering, École Polytechnique Fédérale de Lausanne (EPFL), 1015, Lausanne, Switzerland

* e-mail: chenlu@sari.ac.cn, paul.dyson@epfl.ch, ryan.wang@ucl.ac.uk

This PDF file includes:

Figs. S1 to S20
Tables S1

Contents

Fig. S1. STEM images and particle size distribution of Co _B Cu/Al ₂ O ₃ before reaction.	3
Fig. S2. STEM images and particle size distribution of Co _H Cu/Al ₂ O ₃ before reaction.	4
Fig. S3. STEM images and particle size distribution of Co _B Cu/Al ₂ O ₃ after reaction.	5
Fig. S4. STEM images and particle size distribution of Co _H Cu/Al ₂ O ₃ after reaction..	6
Fig. S5. Compositional elemental mapping of Co _B Cu/Al ₂ O ₃	7
Fig. S6. Electron paramagnetic resonance (EPR) spectra.....	8
Fig. S7. X-Ray diffraction (XRD) patterns and XPS spectra.	9
Fig. S8. Hydrogen temperature-programmed reduction (H ₂ -TPR).	10
Fig. S9. EXAFS fitting of Cu foil and Co foil.	11
Fig. S10. EXAFS fitting of Co _B Cu/Al ₂ O ₃	12
Fig. S11. EXAFS fitting of Co _H Cu/Al ₂ O ₃	13
Fig. S12. Performance of the catalysts in the oxidation of NH ₃ at different temperatures. a Co _B Cu/Al ₂ O ₃ and b Co _H Cu/Al ₂ O ₃	14
Fig. S13. Performance of the catalysts in the oxidation of NH ₃ at different temperatures.....	15
Fig. S14. Performance of Co _B Cu/Al ₂ O ₃ with different Co loading in the oxidation of NH ₃ at different temperatures.	16
Fig. S15. <i>Operando</i> Cu K-edge EXAFS spectra at different reaction temperatures.	17
Fig. S16. <i>Operando</i> Co K-edge EXAFS spectra at different reaction temperatures.	18
Fig. S17. <i>Operando</i> Cu K-edge XANES spectra of different catalysts under different gases.	19
Fig. S18. <i>Operando</i> Cu K-edge EXAFS spectra in different gases.....	20
Fig. S19. <i>Operando</i> Co K-edge EXAFS spectra in different gases.	21
Fig. S20. Cu L-edge (in Auger electron yield (AEY) mode) of Cu foil, Cu ₂ O and CuO.....	22
Table S1. EXAFS fitting results.	23

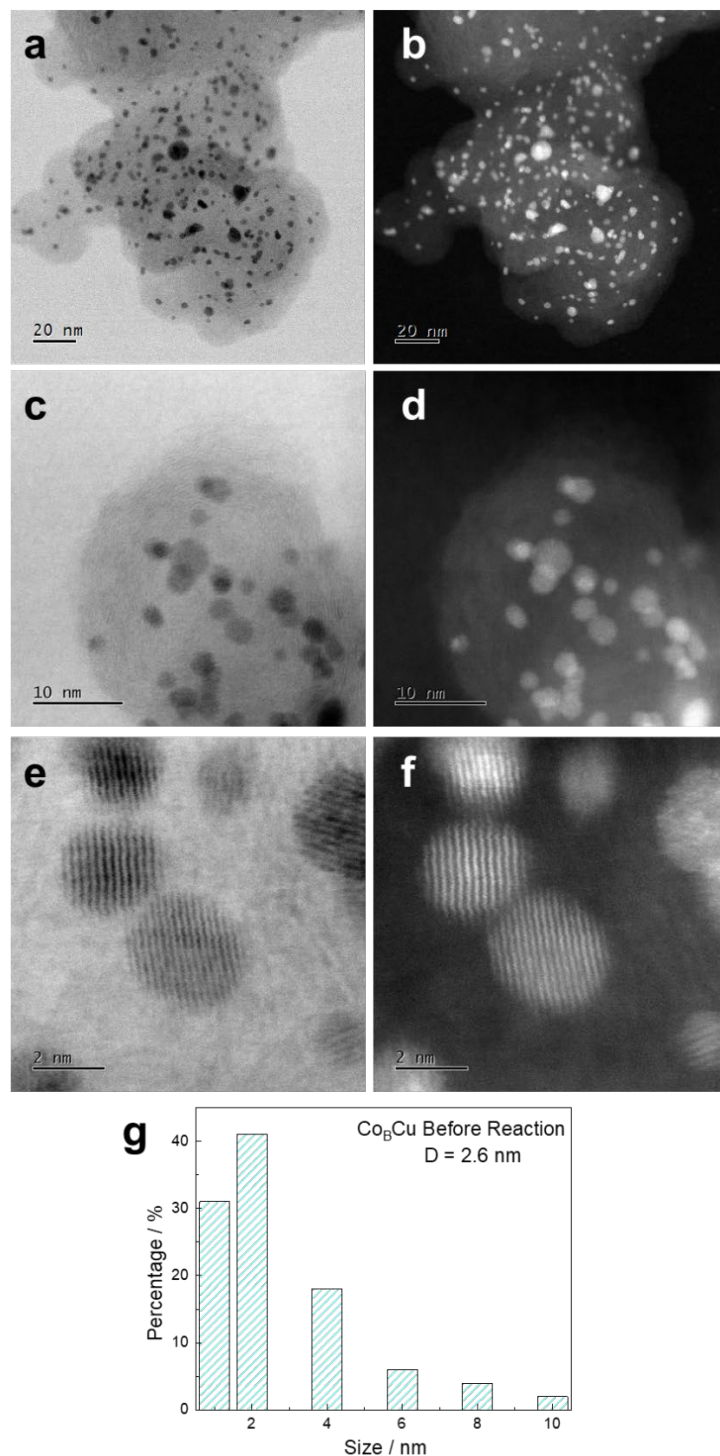


Fig. S1. STEM images and particle size distribution of $\text{Co}_B\text{Cu}/\text{Al}_2\text{O}_3$ before reaction. BF-STEM (a, c, e) and HAADF-STEM (b, d, f) images of $\text{Co}_B\text{Cu}/\text{Al}_2\text{O}_3$ before reaction at different magnifications and the particle size distribution (g). The average particle size was calculated based on more than 100 particles.

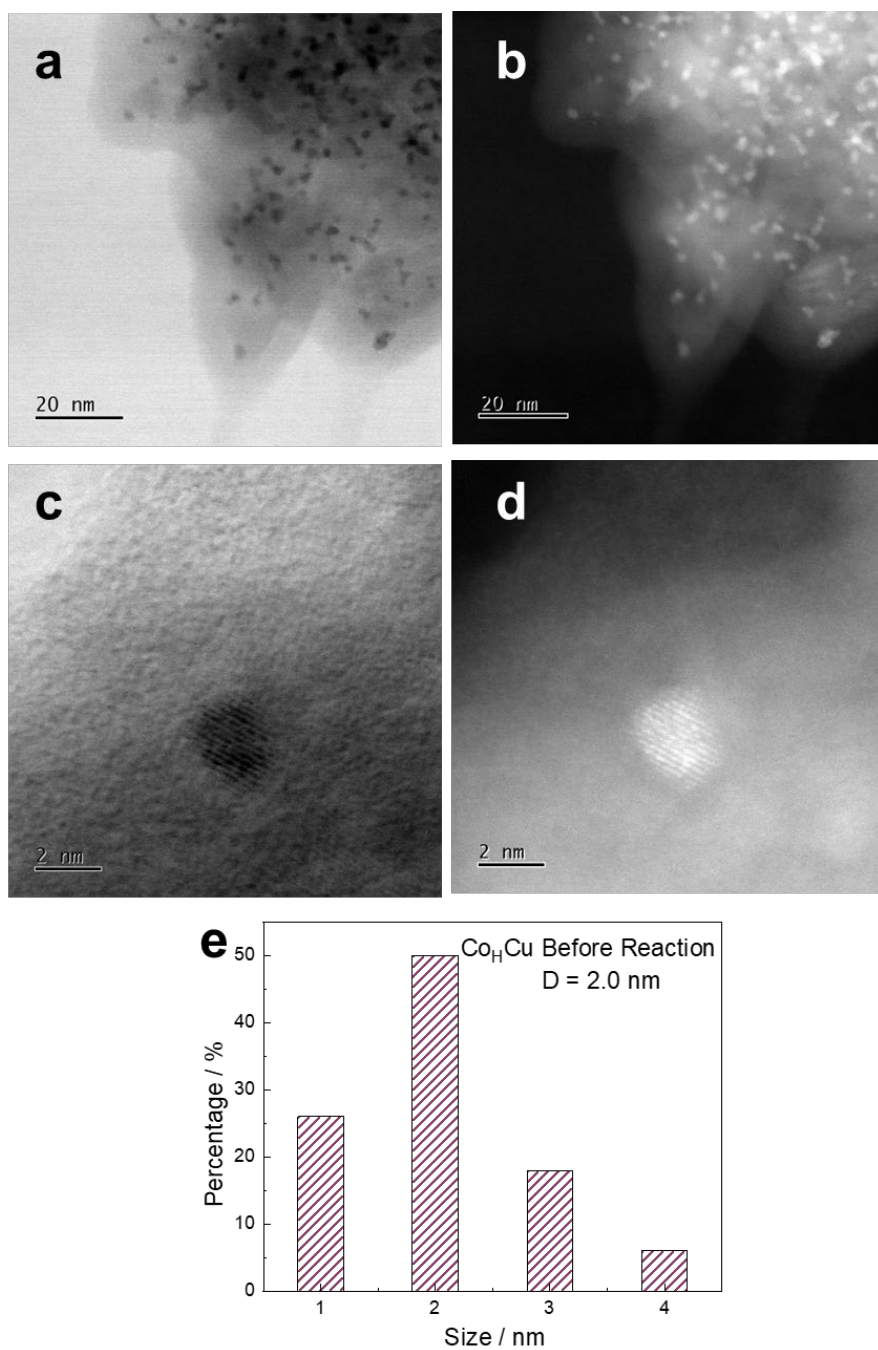


Fig. S2. STEM images and particle size distribution of $\text{Co}_\text{H}\text{Cu}/\text{Al}_2\text{O}_3$ before reaction. BF-STEM (a, c) and HAADF-STEM (b, d) images of $\text{Co}_\text{B}\text{Cu}/\text{Al}_2\text{O}_3$ before reaction at different magnifications and the particle size distribution (e). The average particle size was calculated based on more than 100 particles.

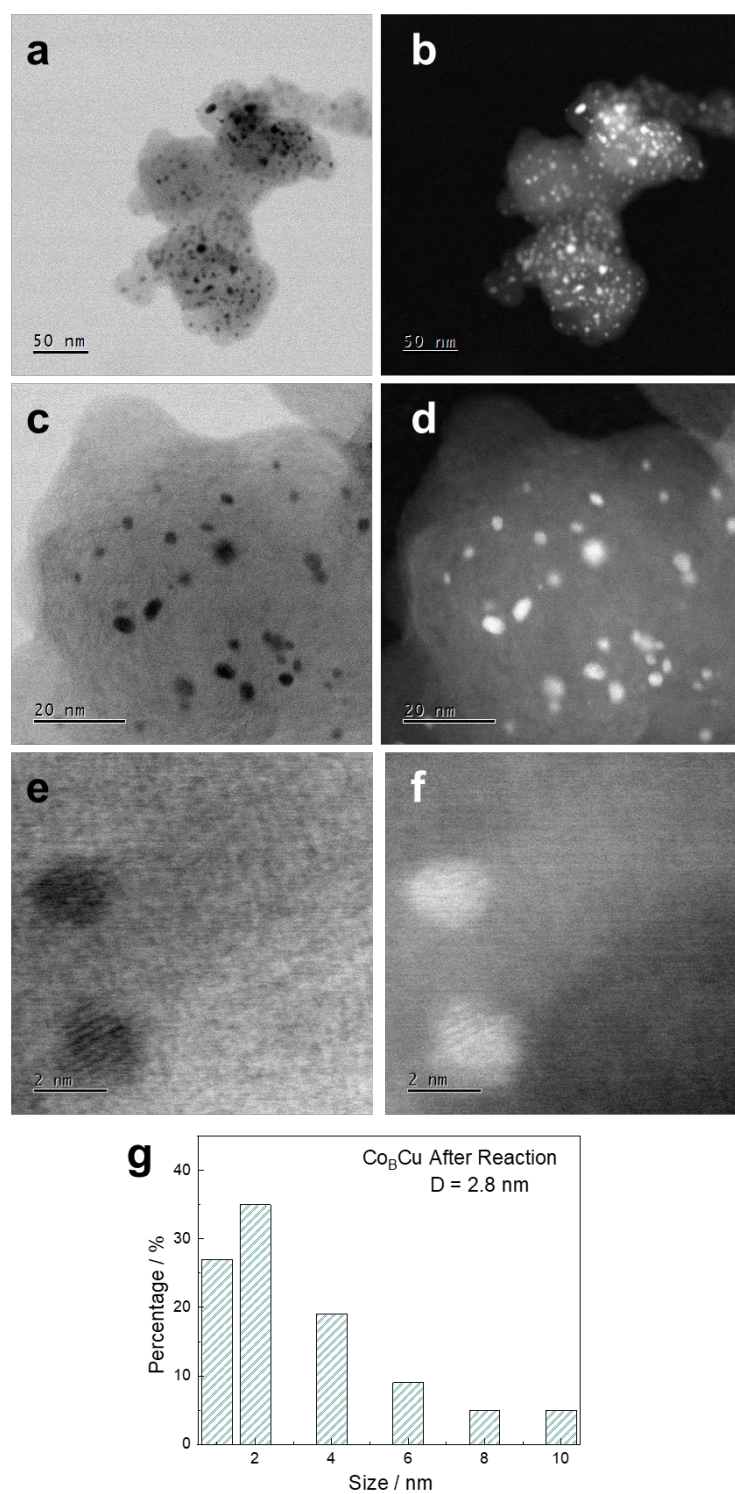


Fig. S3. STEM images and particle size distribution of $\text{Co}_\text{B}\text{Cu}/\text{Al}_2\text{O}_3$ after reaction. BF-STEM (a, c, e) and HAADF-STEM (b, d, f) images of $\text{Co}_\text{B}\text{Cu}/\text{Al}_2\text{O}_3$ before reaction at different magnifications and the particle size distribution (g). The average particle size was calculated based on more than 100 particles.

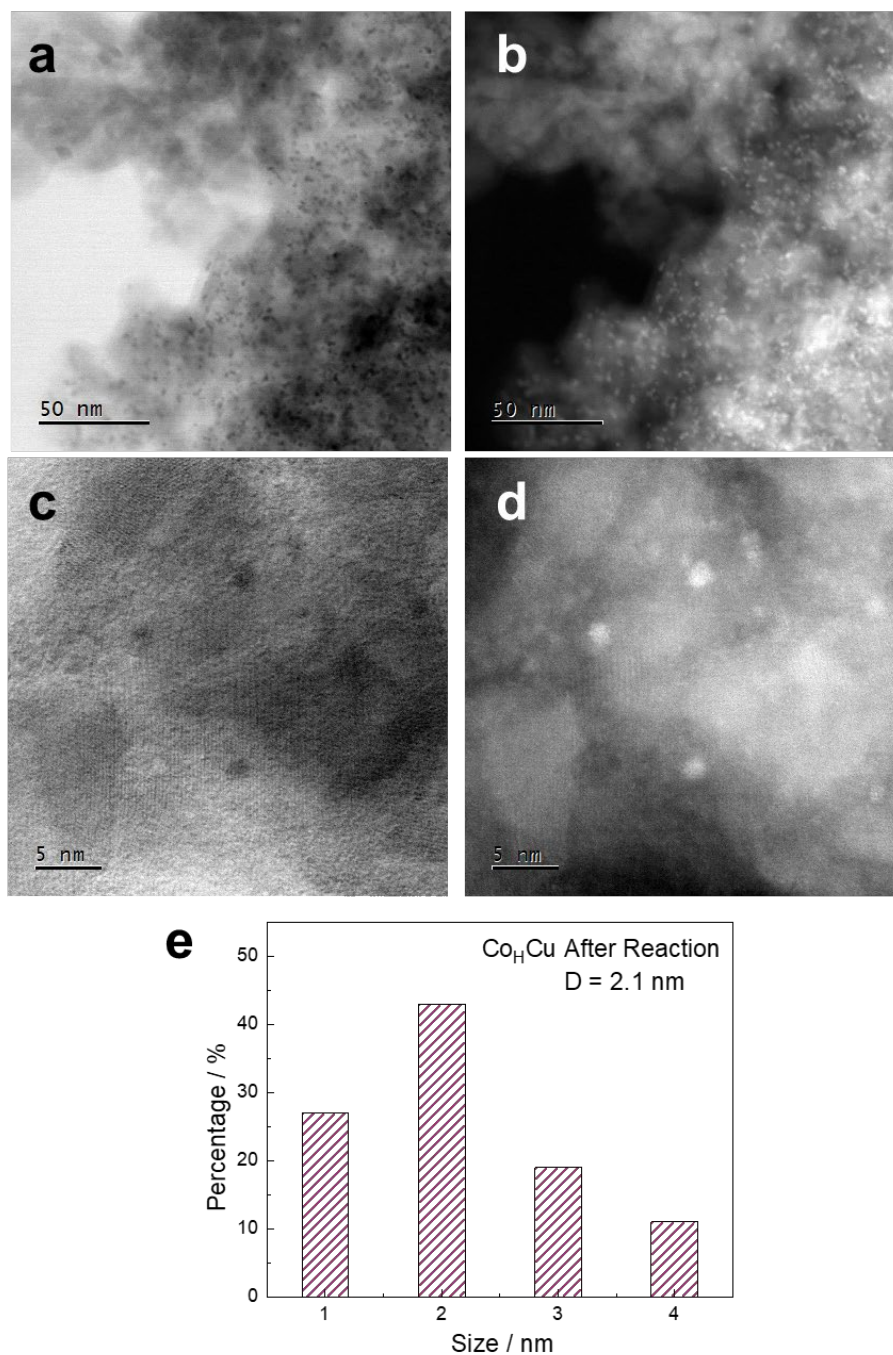


Fig. S4. STEM images and particle size distribution of $\text{Co}_\text{H}\text{Cu}/\text{Al}_2\text{O}_3$ after reaction. BF-STEM (a, c) and HAADF-STEM (b, d) images of $\text{Co}_\text{B}\text{Cu}/\text{Al}_2\text{O}_3$ before reaction at different magnifications and the particle size distribution (e). The average particle size was calculated based on more than 100 particles.

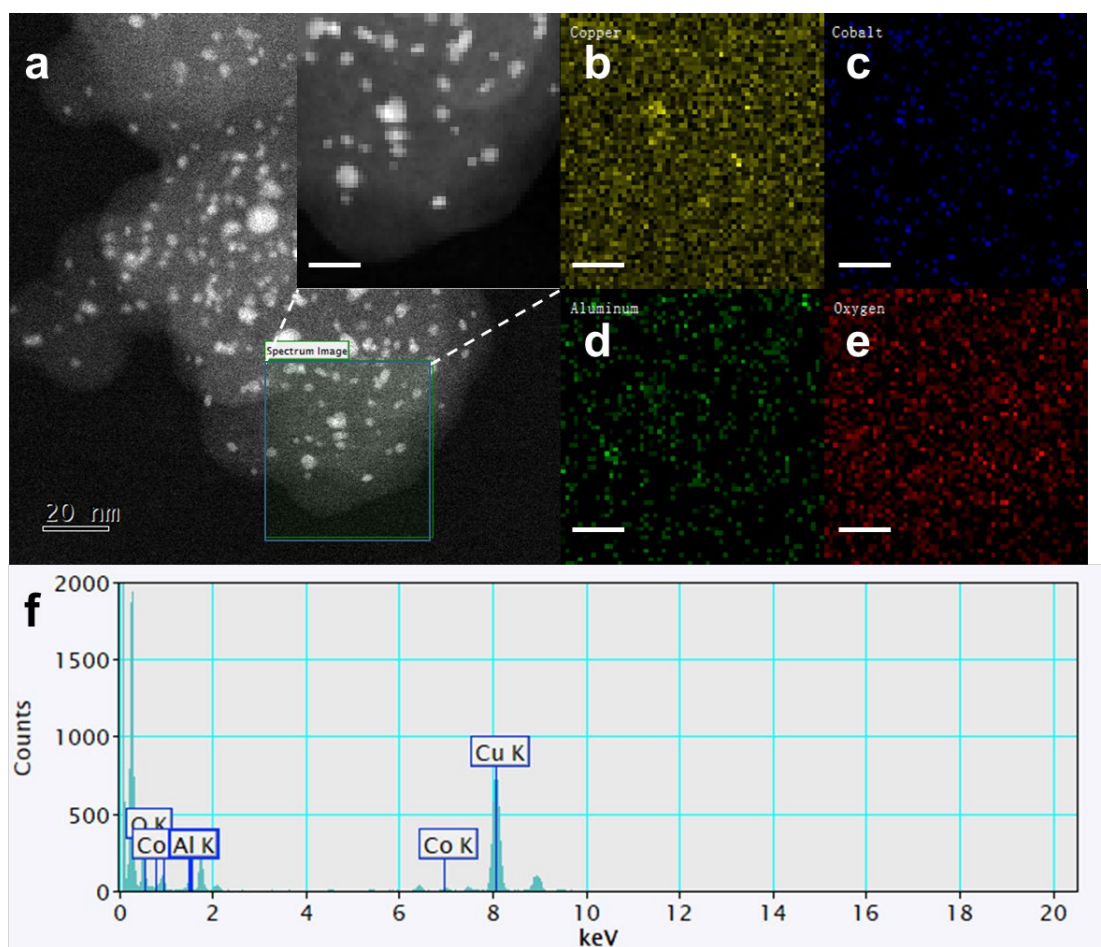


Fig. S5. Compositional elemental mapping of $\text{Co}_B\text{Cu}/\text{Al}_2\text{O}_3$. **a** STEM image of $\text{Co}_B\text{Cu}/\text{Al}_2\text{O}_3$ (inserted image: EDS mapping area, scale bar: 10 nm); **b-e** EDS elemental mapping of $\text{Co}_B\text{Cu}/\text{Al}_2\text{O}_3$ (scale bar: 10 nm); **f** EDX element distribution pattern.

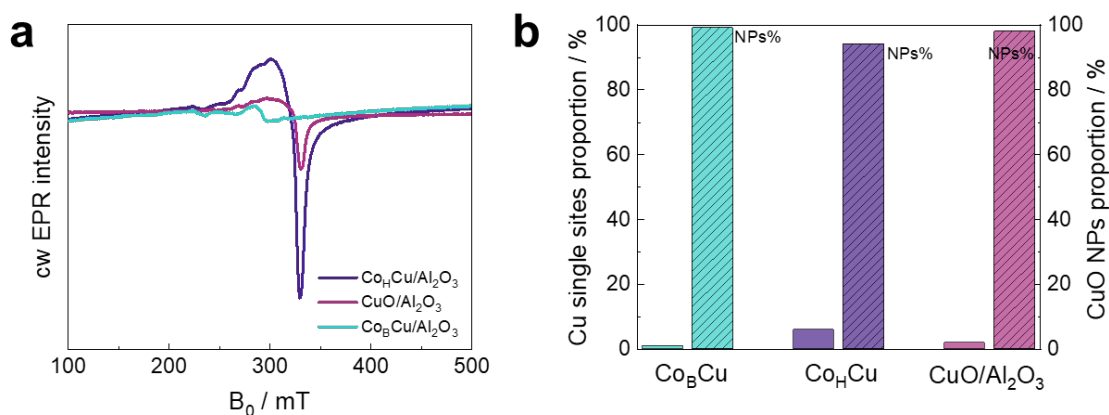


Fig. S6. Electron paramagnetic resonance (EPR) spectra. a EPR spectra of $\text{Co}_\text{B}\text{Cu}/\text{Al}_2\text{O}_3$, $\text{Co}_\text{H}\text{Cu}/\text{Al}_2\text{O}_3$ and $\text{CuO}/\text{Al}_2\text{O}_3$; **b** proportion of Cu single sites and CuO nanoparticles.

EPR spectroscopy: Experiments were performed in continuous-wave (cw) mode on a Bruker E580 X-band EPR spectrometer equipped with a Bruker ER4122-SHQE cavity. Then, 20 mg powder of each sample was loaded into a high-purity quartz EPR tube (4.0 mm o.d., 3.0 mm i.d.) for measurements. All cw EPR spectra were acquired at room temperature over a wide magnetic field range. Typical spectrometer parameters were sweep time (300 s), center field (300 mT), sweep width (300 mT), modulation frequency (100 kHz), microwave frequency (9.87 GHz), and microwave power (2.0 mW).

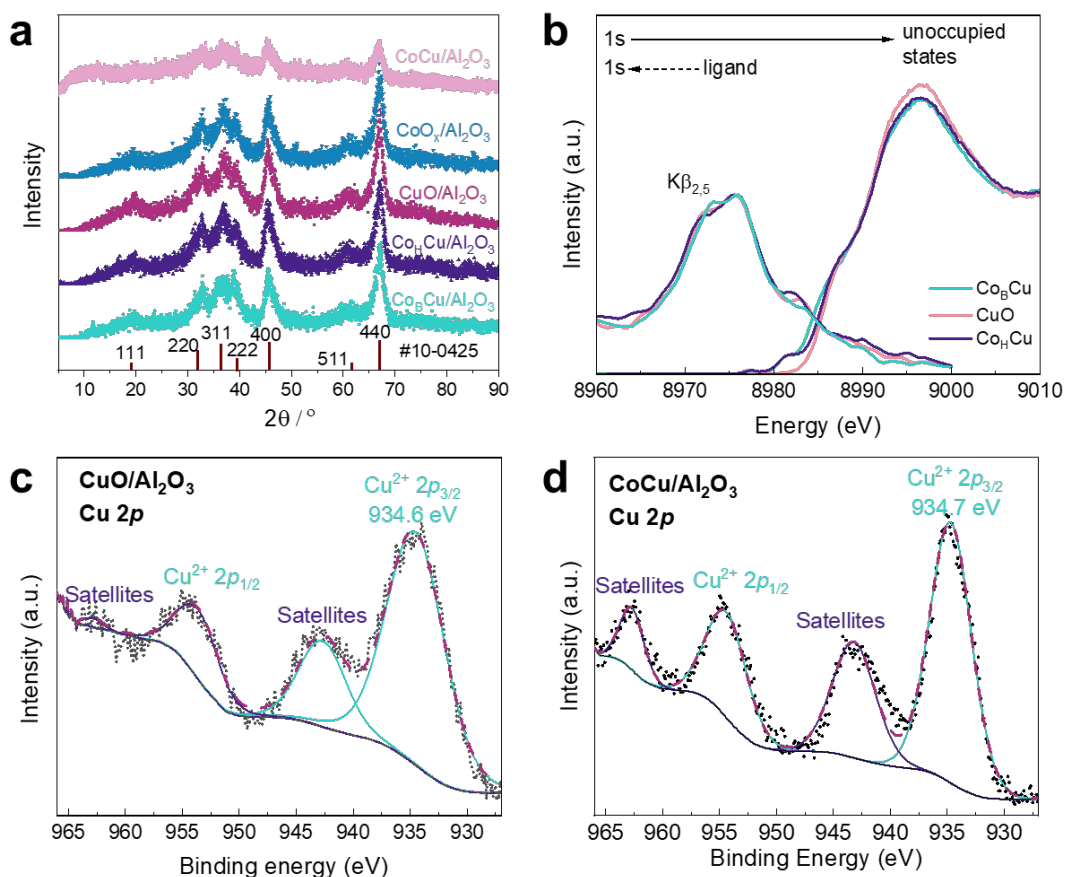


Fig. S7. X-Ray diffraction (XRD) patterns and XPS spectra. **a** XRD patterns of $\text{CoO}_x/\text{Al}_2\text{O}_3$, $\text{CuO}/\text{Al}_2\text{O}_3$, $\text{Co}_B\text{Cu}/\text{Al}_2\text{O}_3$ and $\text{Co}_H\text{Cu}/\text{Al}_2\text{O}_3$. JCPDS card number of $\gamma\text{-Al}_2\text{O}_3$: #10-0425 (Peaks at $2\theta = 19.2, 32.0, 36.6, 39.3, 46, 61.5$ and 67° , are indexed as the (111), (220), (311), (222), (400), (511) and (440) reflections of $\gamma\text{-Al}_2\text{O}_3$.); **b** VtC and XANES of $\text{CuO}/\text{Al}_2\text{O}_3$, $\text{Co}_B\text{Cu}/\text{Al}_2\text{O}_3$ and $\text{Co}_H\text{Cu}/\text{Al}_2\text{O}_3$; $\text{Cu } 2p$ XPS spectra of $\text{CuO}/\text{Al}_2\text{O}_3$ (**c**) and $\text{CoCu}/\text{Al}_2\text{O}_3$ (**d**).

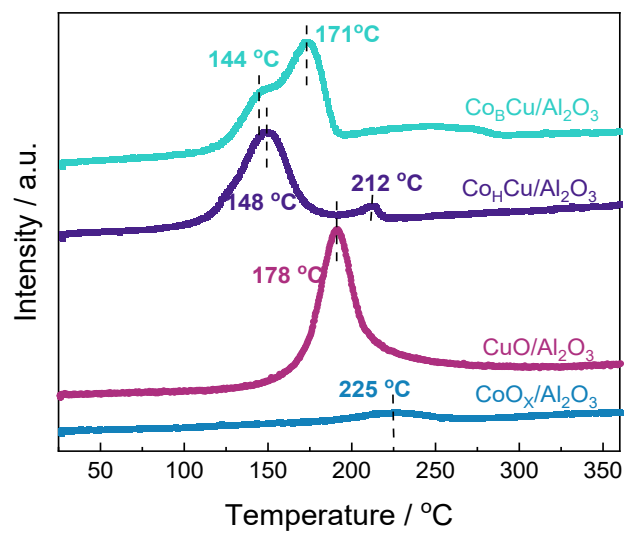


Fig. S8. Hydrogen temperature-programmed reduction (H₂-TPR). H₂-TPR of CoO_x/Al₂O₃, CuO/Al₂O₃, Co_BCu/Al₂O₃ and Co_HCu/Al₂O₃.

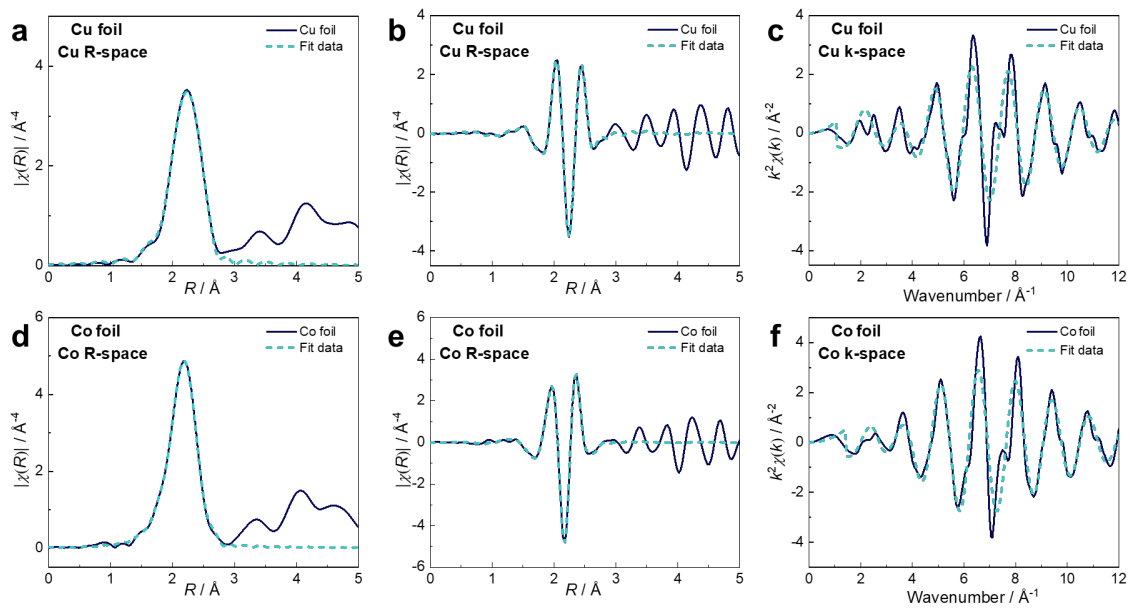


Fig. S9. EXAFS fitting of Cu foil and Co foil. EXAFS fitting results of Cu K-edge of Cu foil (a-c) and Co K-edge of Co foil (d-f) in R-space, R-space (without phase correction) and k-space.

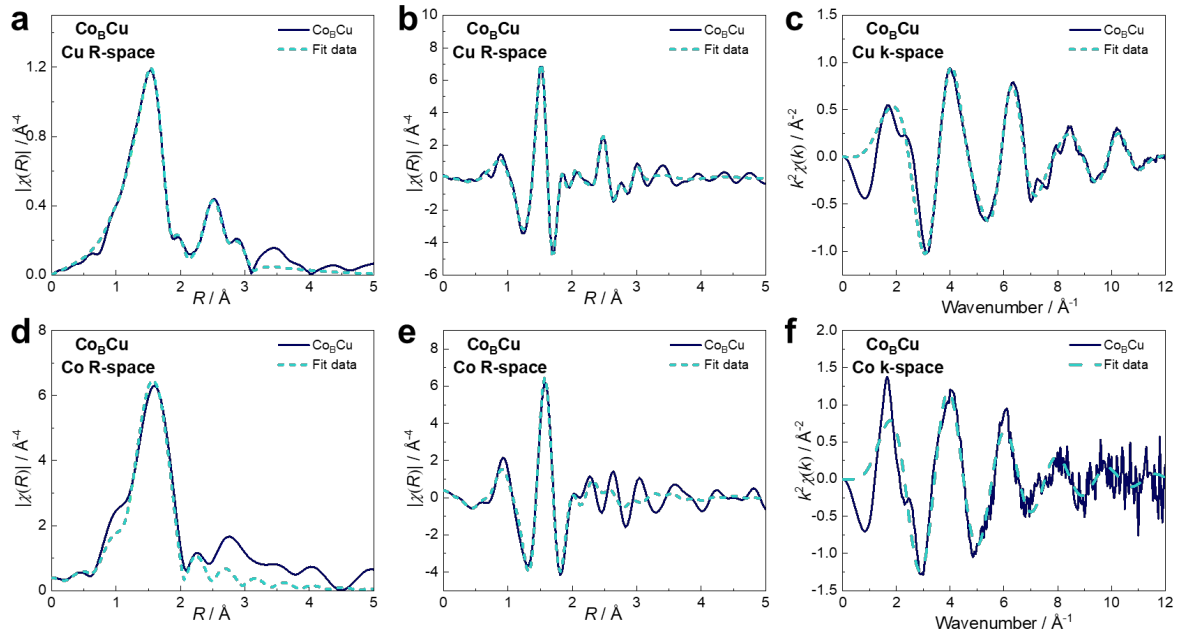


Fig. S10. EXAFS fitting of Co_BCu/Al₂O₃. EXAFS fitting results of Cu K-edge (a-c) and Co K-edge (d-f) of Co_BCu/Al₂O₃ in R-space, R-space (without phase correction) and k-space.

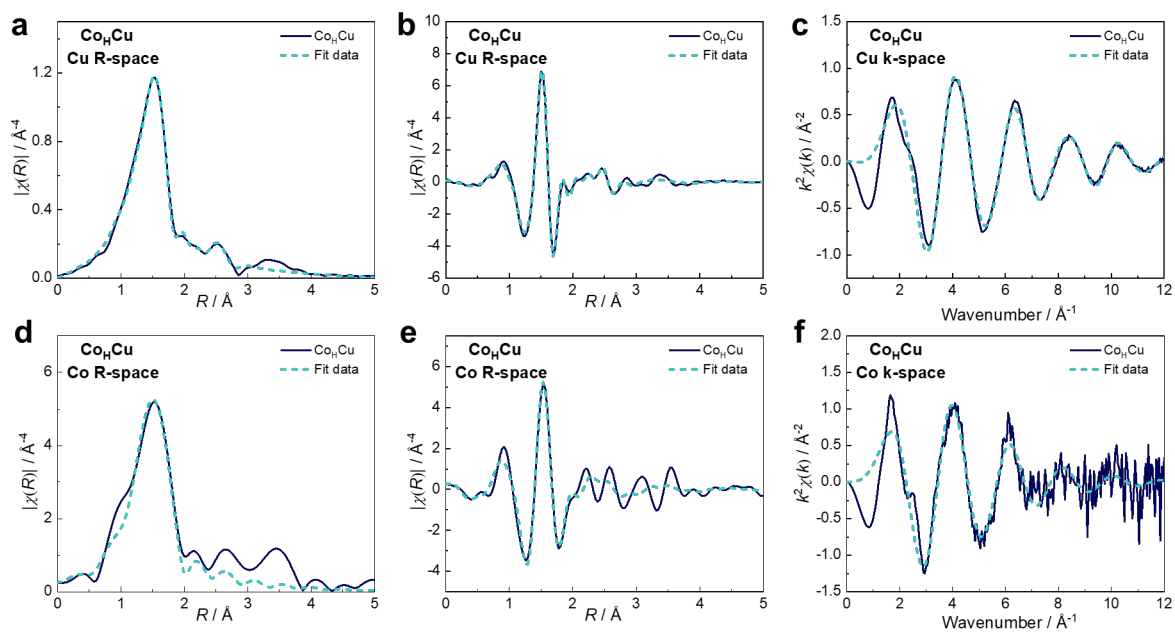


Fig. S11. EXAFS fitting of $\text{Co}_\text{H}\text{Cu}/\text{Al}_2\text{O}_3$. EXAFS fitting results of Cu K-edge (a-c) and Co-K edge (d-f) and $\text{Co}_\text{H}\text{Cu}/\text{Al}_2\text{O}_3$ in R-space, R-space (without phase correction) and k-space.

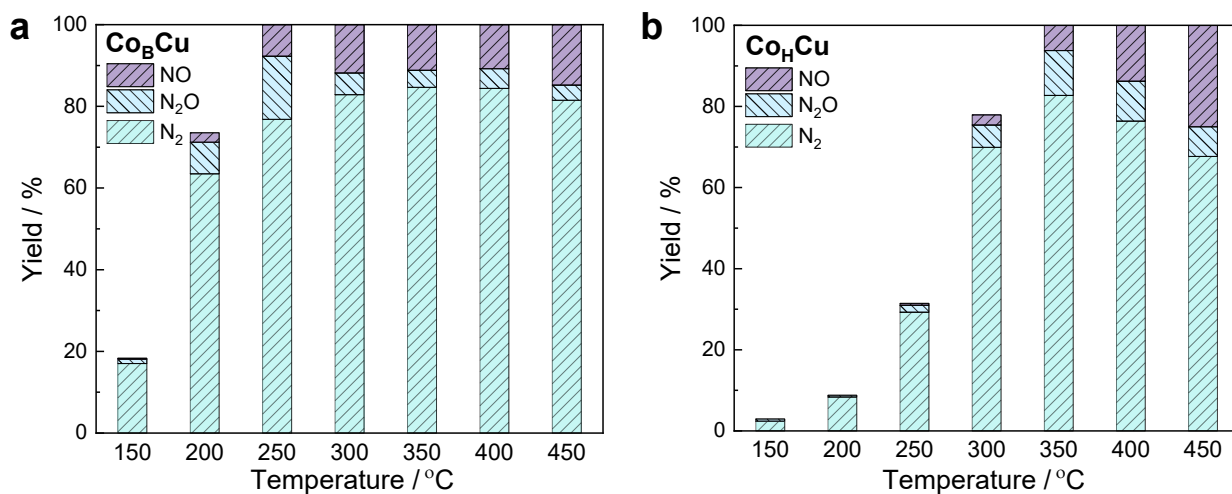


Fig. S12. Performance of the catalysts in the oxidation of NH₃ at different temperatures. a Co_BCu/Al₂O₃ and **b** Co_HCu/Al₂O₃. (Reaction conditions: 50 mg catalyst, 5000 ppm NH₃, 5% O₂ balanced in He, gas flow: 100 mL/min).

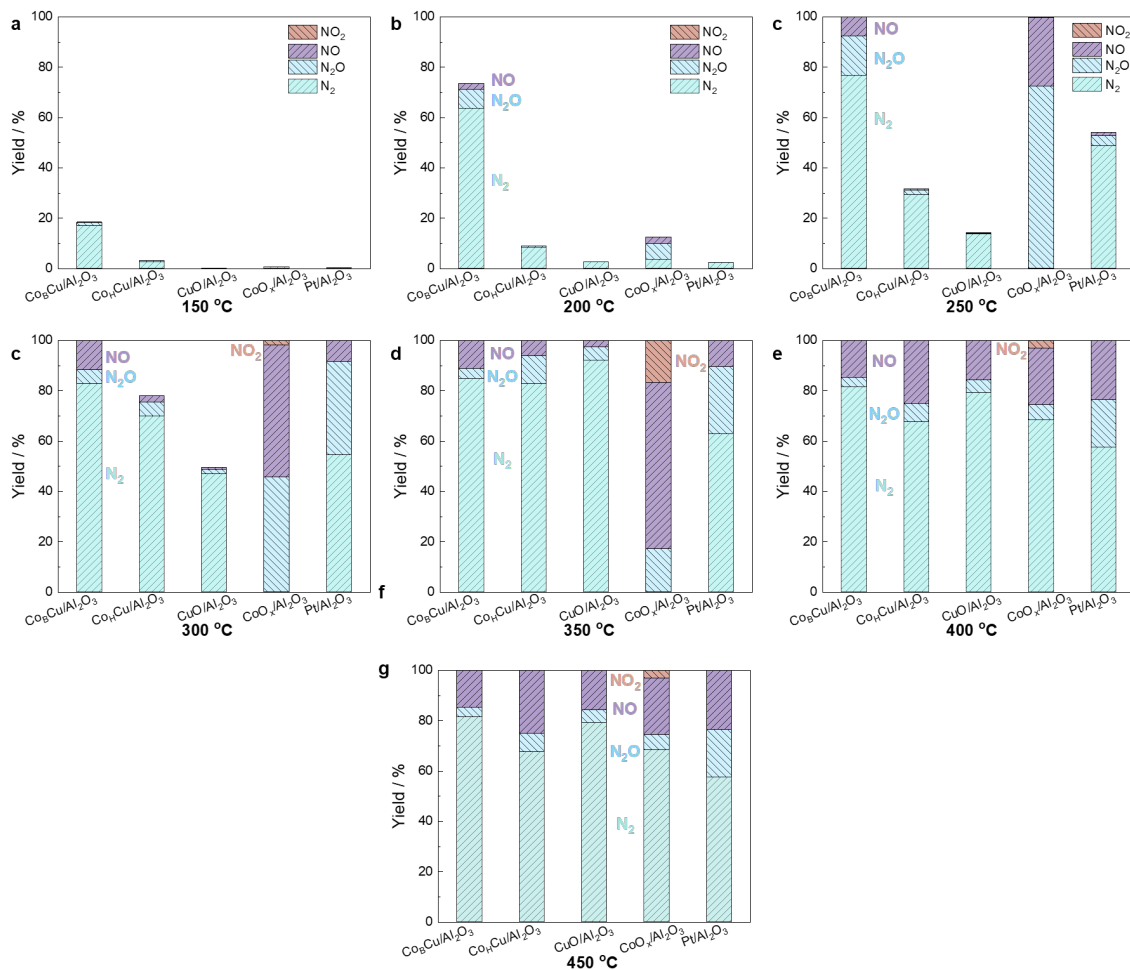


Fig. S13. Performance of the catalysts in the oxidation of NH_3 at different temperatures. a 150 °C, b 200 °C, c 250 °C, d 300 °C, e 350 °C, f 400 °C, g 450 °C. (Reaction conditions: 50 mg catalyst, 5000 ppm NH_3 , 5% O_2 balanced in He, gas flow: 100 mL/min).

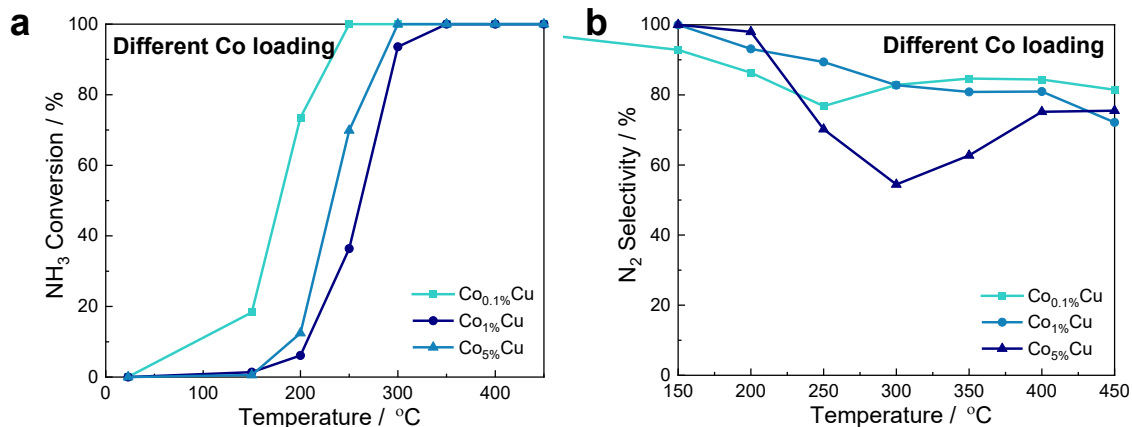


Fig. S14. Performance of $\text{Co}_\text{B}\text{Cu}/\text{Al}_2\text{O}_3$ with different Co loading in the oxidation of NH_3 at different temperatures. a Conversion of NH_3 , **b** selectivity to N_2 . (Reaction conditions: 50 mg catalyst, 5000 ppm NH_3 , 5% O_2 balanced in He, gas flow: 100 mL/min).

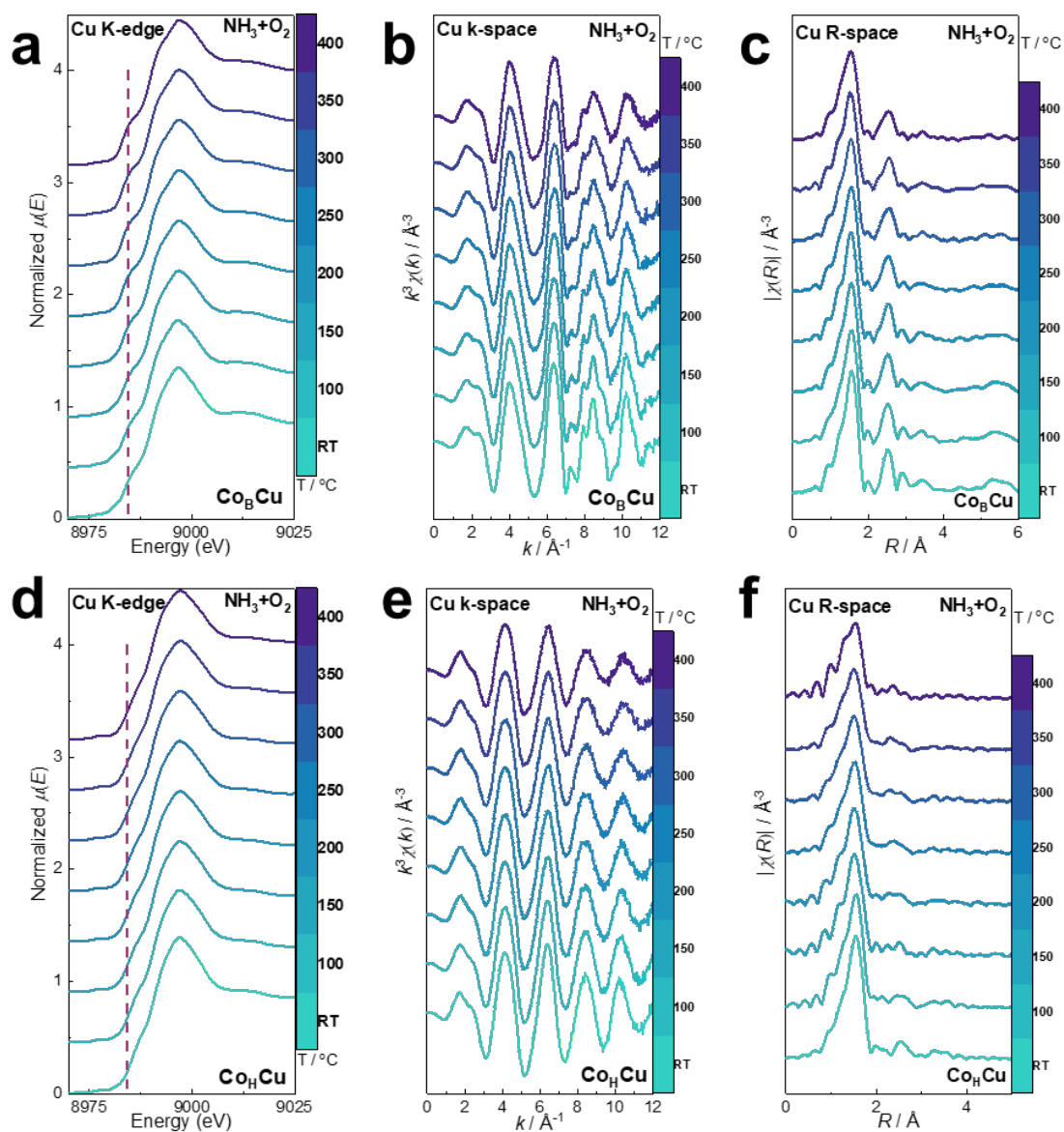


Fig. S15. Operando Cu K-edge EXAFS spectra at different reaction temperatures. Operando EXAFS Cu K-edge, k-space and R-space of $\text{Co}_\text{B}\text{Cu}/\text{Al}_2\text{O}_3$ (**a, b, c**) and $\text{Co}_\text{H}\text{Cu}/\text{Al}_2\text{O}_3$ (**d, e, f**) as a function of temperature.

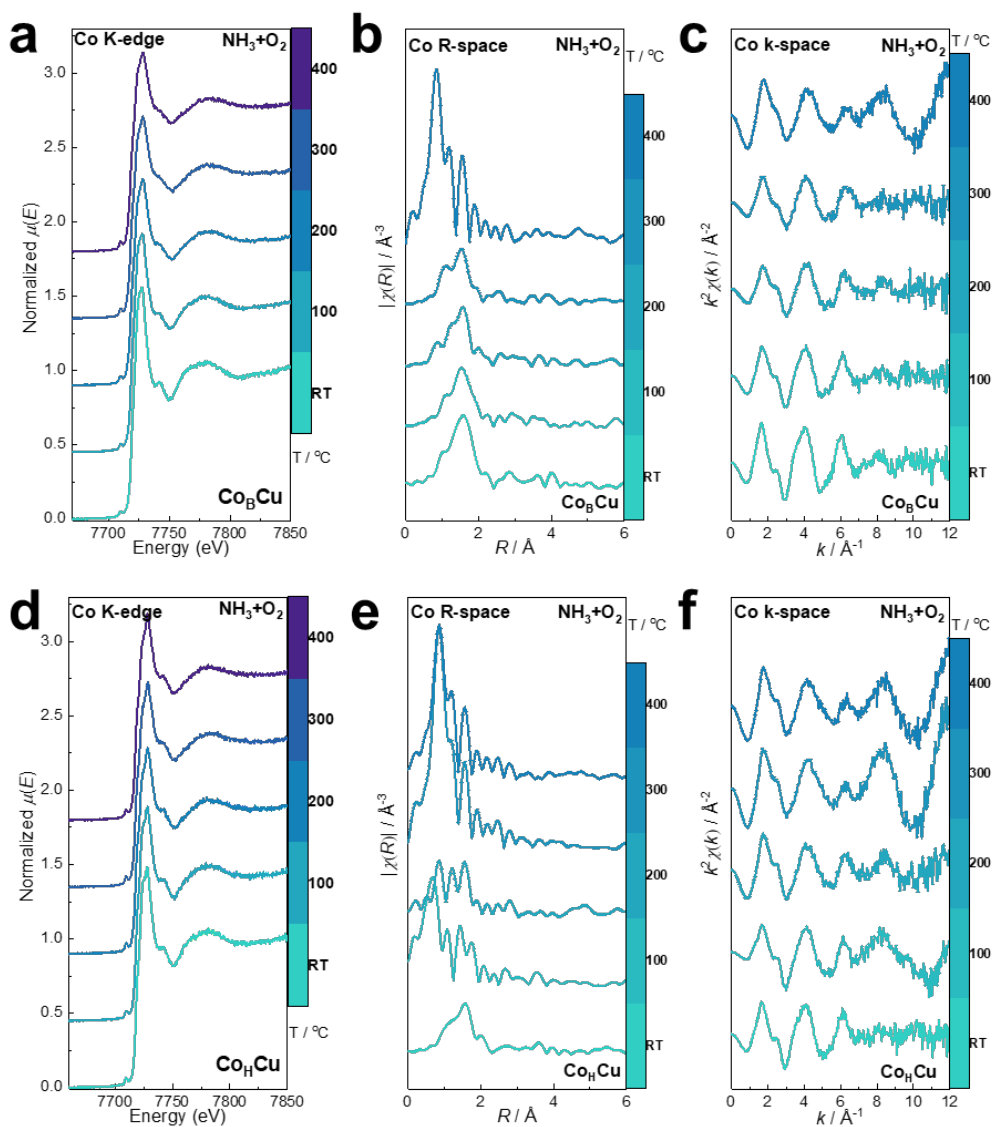


Fig. S16. Operando Co K-edge EXAFS spectra at different reaction temperatures. Operando EXAFS Co K-edge, R-space and k-space of $\text{Co}_\text{B}\text{Cu}/\text{Al}_2\text{O}_3$ (a, b, c) and $\text{Co}_\text{H}\text{Cu}/\text{Al}_2\text{O}_3$ (d, e, f) as a function of temperature.

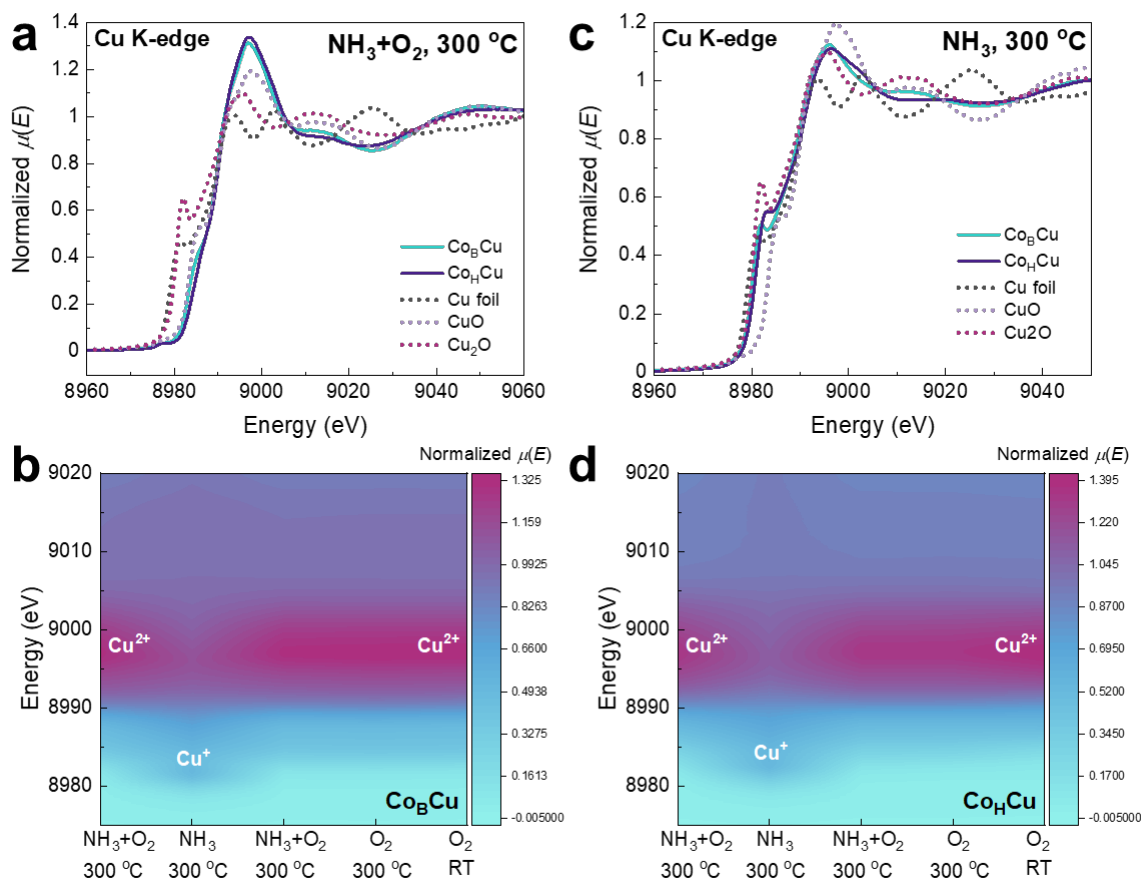


Fig. S17. Operando Cu K-edge XANES spectra of different catalysts under different gases. Operando XANES Cu K-edge of $\text{Co}_B\text{Cu}/\text{Al}_2\text{O}_3$ and $\text{Co}_H\text{Cu}/\text{Al}_2\text{O}_3$ in NH_3+O_2 at 300°C (a) or in NH_3+O_2 at 300°C (b); 2D XAFS maps of $\text{Co}_B\text{Cu}/\text{Al}_2\text{O}_3$ (c) and $\text{Co}_H\text{Cu}/\text{Al}_2\text{O}_3$ (d) in different gases.

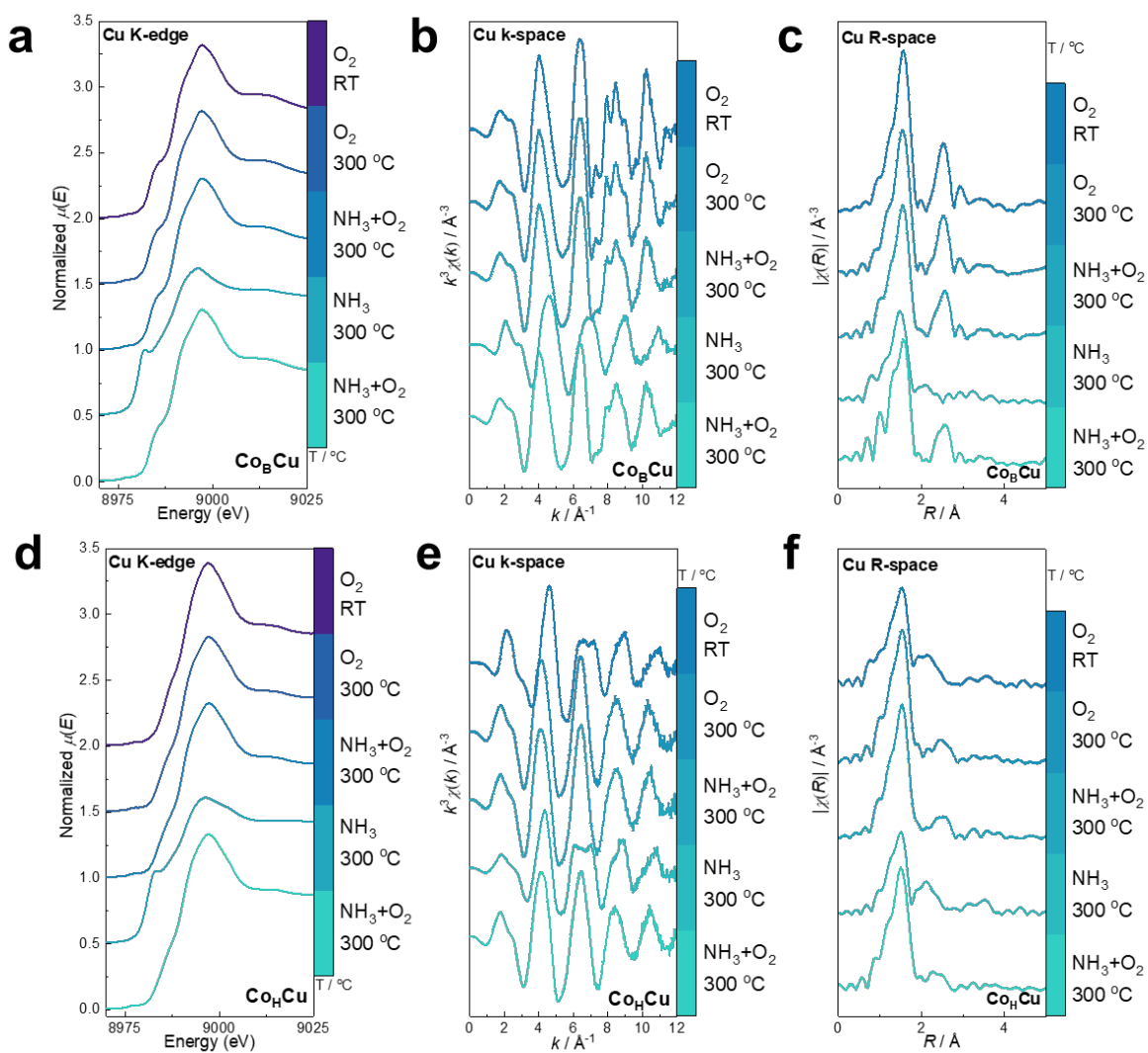


Fig. S18. Operando Cu K-edge EXAFS spectra in different gases. In-situ EXAFS Cu K-edge, k-space and R-space of $\text{Co}_\text{B}\text{Cu}/\text{Al}_2\text{O}_3$ (a, b, c) and $\text{Co}_\text{H}\text{Cu}/\text{Al}_2\text{O}_3$ (d, e, f) in different gases.

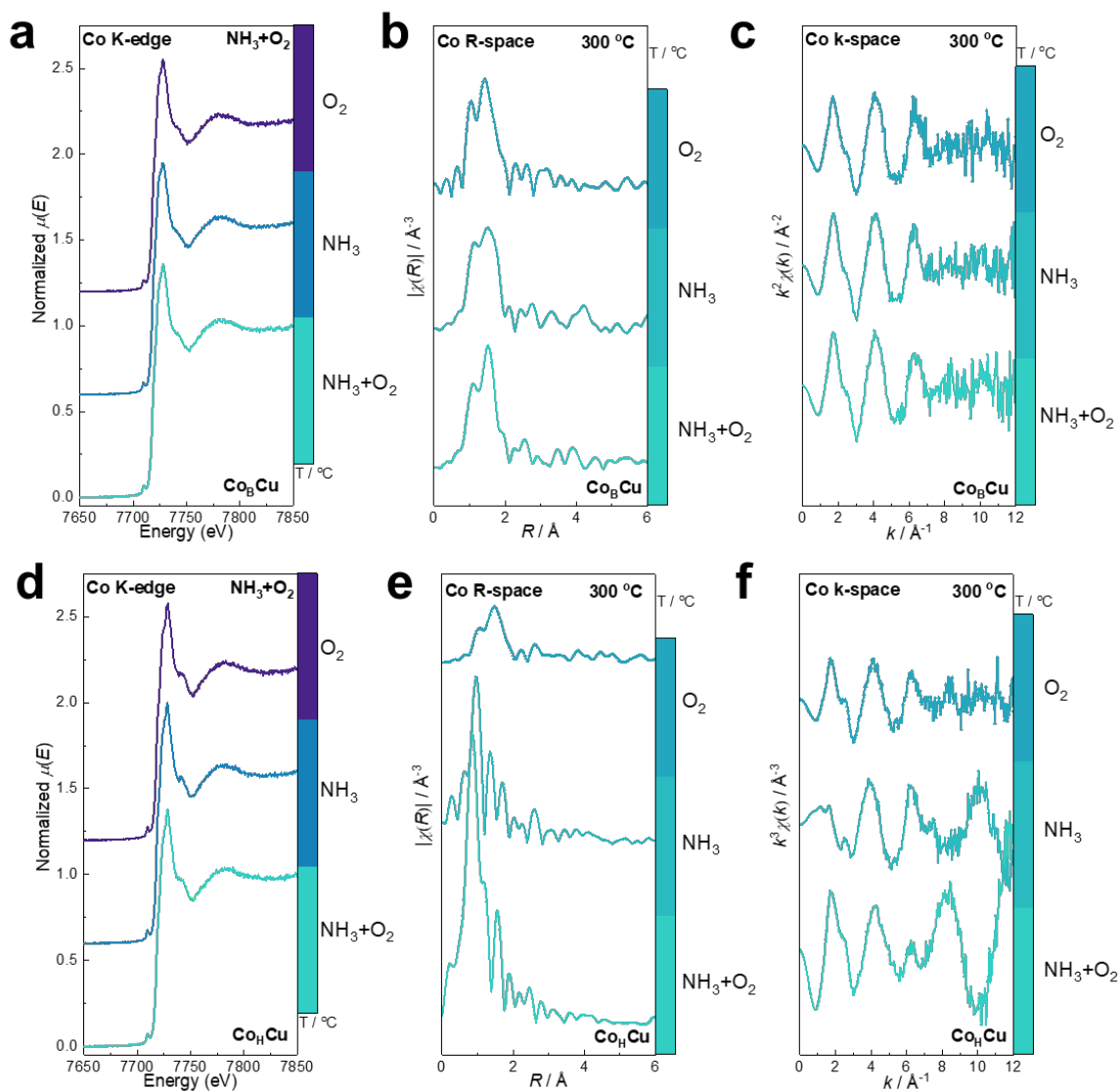


Fig. S19. Operando Co K-edge EXAFS spectra in different gases. Operando EXAFS Co K-edge, R-space and k-space of Co_BCu/Al₂O₃ (a, b, c) and Co_HCu/Al₂O₃ (d, e, f) in different gases.

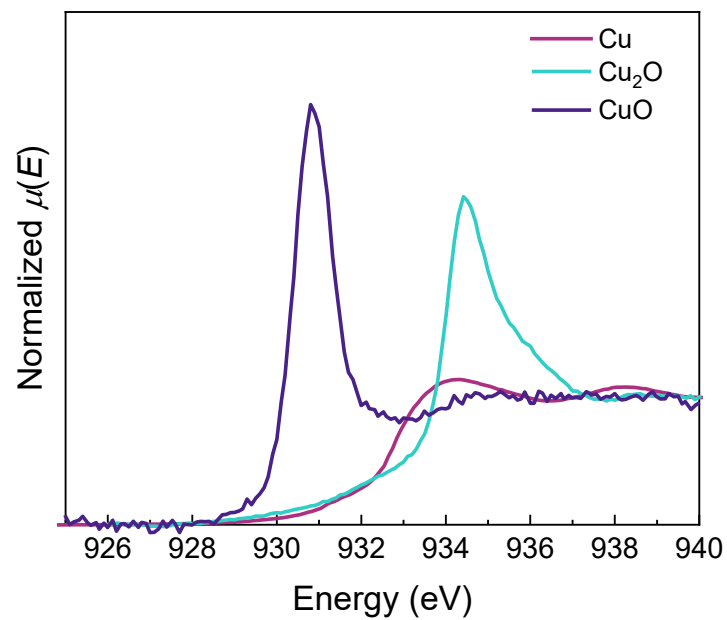


Fig. S20. Cu L-edge of Cu foil, Cu₂O and CuO. It is in Auger electron yield (AEY) mode.

Table S1. EXAFS fitting results.

Sample	Scattering	C.N.	d (Å)	σ^2	R-factor	E_0 (eV)
Cu foil STD	Cu-Cu	12	2.56			
Cu ₂ O STD	Cu-O	2	1.85			
	Cu-Cu	12	3.01			
CuO STD	Cu-O	4	1.95			
		4	2.88			
	Cu-Cu	4	3.07			
		2	3.16			
Co foil STD	Co-Co	12	2.50			
Co _B Cu/Al ₂ O ₃	Cu-O	3.45 ± 0.12	1.96 ± 0.005	0.005 ± 0.0005	0.003	-0.42 ± 0.42
	Cu-Cu(1)	2.39 ± 0.48	2.91 ± 0.03	0.009 ± 0.002		
	Cu-Cu(2)	1.90 ± 0.39	3.10 ± 0.03	0.009 ± 0.002		
Co _B Cu/Al ₂ O ₃	Co-O	5.74 ± 0.99	2.04 ± 0.0002	0.008 ± 0.003	0.013	-0.51 ± 1.97
	Co-Co	-	-	-		
Co _H Cu/Al ₂ O ₃	Cu-O	3.33 ± 0.12	1.93 ± 0.003	0.005 ± 0.0005	0.004	-0.77 ± 0.50
	Cu-Cu (1)	0.22 ± 0.21	2.91 ± 0.021	0.005 ± 0.007		
	Cu-Cu (2)	-	-	-		
Co _H Cu/Al ₂ O ₃	Co-O	5.92 ± 1.09	1.99 ± 0.004	0.010 ± 0.003	0.019	-2.95 ± 2.14
	Co-Co	-	-	-		